Residual Stress in Nanocrystalline Nickel Tungsten Electrodeposits

by

Tiffany D. Ziebell

B.S., Materials Science and Engineering
Northwestern University, 2005

SUBMITTED TO THE DEPARTMENT OF MATERIALS SCIENCE AND ENGINEERING
IN PARTIAL FULFILLMENT OF THE REQUIREMENTS FOR THE DEGREE OF

MASTER OF SCIENCE IN MATERIALS SCIENCE AND ENGINEERING
AT THE
MASSACHUSETTS INSTITUTE OF TECHNOLOGY

September 2011

Author.....
Department of Materials Science and Engineering
August 4th, 2011

Certified by.....
Christopher A. Schuh
Danae and Vasilios Salapatas Professor of Metallurgy
Thesis Supervisor

Accepted by.....
Christopher A. Schuh
Chairman, Departmental Committee on Graduate Students

Residual Stress in Nanocrystalline Nickel-Tungsten Electrodeposits

by

Tiffany D. Ziebell

Submitted to the Department of Materials Science and Engineering on
August 5, 2011 in Partial Fulfillment of the Requirements for the
Degree of Master of Science in Materials Science and Engineering

ABSTRACT

Characterizing the residual stress of thick nanocrystalline electrodeposits poses several unique challenges due to their fine grain structure, thickness distribution, and matte surface. We employ a three-dimensional profilometry-based approach that addresses each of these complicating factors and enables quantitative analysis of residual stress with reasonable accuracy. The specific emphasis of this work is thick (10-100 μm), nanocrystalline Ni-W electrodeposits, in which residual stresses arise during the deposition process as well as during post-deposition annealing. The present measurements (for grain sizes ranging from 4-63 nm) offer quantitative insight into the mechanisms of stress development and evolution in these alloys, suggesting that the grain boundary structure is out of equilibrium (unrelaxed) and contains excess free volume, in and of itself acting as the primary source of residual stress in these coatings. We show that the amount of free volume initially created in the films can be predicted from the pulse amplitude of the current waveform employed during the deposition process while the corresponding grain size dictates the volume fraction of grain boundary area where this free volume can be accommodated – together, these processing and structure-based parameters control the resulting stress level in the film.

Thesis Supervisor: Christopher A. Schuh
Title: Danae and Vasilios Salapatas Associate Professor of Metallurgy

Acknowledgments

First and foremost, I would like to thank my advisor, Chris Schuh, for his endless patience, guidance, and support as I maneuvered along the bumpy road of research and, more importantly, as I slowly shaped my non-traditional career path. I also gratefully acknowledge the insight and wisdom of Ying, Shiyun, Jeremy, Corinne, Tim, and all of the Schuh group members.

I would also like to thank all my friends and family, both near and far, for bringing a healthy balance to my life. And, finally, this thesis work would not have been possible without the unconditional love and support of my husband, Anubhav – to whom I am eternally grateful.

Table of Contents

List of Figures

Figure 7: a) The intrinsic residual stress of the as-deposited Ni-W films ranges from approximately 300-1300 MPa for pulse amplitudes ranging from 0 to 0.5 A/cm^2. b) Re-plotting this data as a function of grain size in a semi-logarithmic fashion better represents the range of accessible grain sizes. A rapid increase in residual stress occurs with an increase in grain size below ~20 nm while further increases in grain size result in a gradual decrease in stress.

Figure 9: a) The increase in residual stress occurring during the annealing process ranges from approximately 300 to 1000 MPa and b) the maximum residual stress of the annealed Ni-W films ranges from approximately 600 to 2400 MPa for grain sizes between 5-60 nm.

Figure 10: Only a slight increase in residual stress (~15-45 MPa) is observed following the removal of co-deposited hydrogen by outgassing under vacuum at 0.2 mbar at room temperature for 22 hours. These results suggest that the post-deposition release of hydrogen plays a very minor role in the final residual stress state of electrodeposited nanocrystalline Ni-W films and would not be responsible for the large volume shrinkage observed following annealing.

Figure 11: (a) The dashed grey curve represents the calculated excess free volume content in the grain boundaries, $F(d)$, which is controlled by the *processing* parameter A_p while the dotted black curve represents the volume fraction of grain boundary area in the film, $V_{gb}(d)$, which is dependent on the *structural* grain size of the film. Multiplying these two terms together yields the red curve, which represents the bulk excess free volume content of the film, $V_{ex}(d)$, and provides a good indicator of the expected increase in residual stress associated with annealing out this excess free volume. Note that $V_{ex}(d)$ has been multiplied by a factor of 30x for ease of visibility. (b) A comparison of the experimentally-determined $\Delta\sigma$ values as a function of grain size with those values calculated using Eqn. 15.

Figure 12: Correlation between the as-deposited residual stress and maximum increase in residual stress upon annealing for the Ni-W films. This relationship points to a similar mechanism of grain boundary free volume also playing a role in the as-deposited stress state.

Figure 13: Experimentally-determined and calculated as-deposited residual stress values for electrodeposited Ni-W films ranging in grain size from approximately 5-60 nm. The as-deposited residual stress results from grain boundary void shrinkage occurring during the deposition process. The amount of free volume created and stored in the grain boundaries during the deposition process is set by both the pulse amplitude, A_p, which determines the amount of free volume (or voids) created and thereby the percentage of grain boundary volume that will be composed of free volume, and the grain size, d, which determines the volume fraction of grain boundary area.

List of Tables

1. Introduction

When the grain size of a material is refined into the nanometer range, a significant volume fraction of atoms are located in the grain boundaries, and the interfaces begin to play a dominant role in shaping both its physical and mechanical properties. The resulting ultra-high yield and fracture strengths, as well as other beneficial properties, observed in nanocrystalline metals have continued to stimulate interest [1-8]. Electrodeposited nanocrystalline Ni-W alloys in particular have found wide application for coatings due to their high hardness, excellent corrosion and wear resistance, and ease of processing [9-12]. However, as with many coating technologies, residual stress in nanocrystalline deposits can lead to detrimental effects including a decrease in fatigue strength, cracking under service conditions, or delamination [13-15]. In advanced electronics and micro-electromechanical systems applications, warping of the underlying fine-scale substrate features can also occur when a coating is applied or upon subsequent thermal treatment [16]. The prospect for component failures due to such internal stress issues continues to be a technology-limiting barrier, and thus understanding their origins and controlling them is of great practical importance.

Despite the significance of residual stress in nanocrystalline coatings of every kind, quantitative measurement of these stresses is experimentally challenging due to the complexities arising from their structure and processing history. For example, whereas X-ray diffraction is a common approach to measure lattice strains, from which stresses are inferred via elasticity theory [17, 18], in nanocrystalline materials this method is often difficult or even impossible to apply. Small grain sizes in combination with microstrains lead to substantial peak broadening and even peak distortion, which can degrade the measurement accuracy of minute shifts in Bragg angles [19,

20]. Moreover, in the finest nanocrystalline alloys, with grain sizes below about 10 nm [10, 12], the diffraction signal is sufficiently broad as to appear more like an amorphous halo rather than the set of discrete crystallographic peaks normally required for accurate stress measurements. In such specimens, the principal reflection is distinguishable, but the higher-order reflections needed for the most accurate stress measurements are usually insufficient for quantitative analysis.

Similarly, the use of the bent-strip test method common in the electrodeposition industry, which relies on measurements of residual-stress-induced substrate deflections [21-23], presents additional challenges for contemporary nanocrystalline electrodeposition methods. This is largely because these methods employ long, cantilevered substrates to produce large, easily measurable deflections, and as a result the anode-cathode distance changes as a function of both time and position as plating proceeds and the substrate gradually warps [19]. An additional issue concerns the use of very thin foil for the substrate in these measurements, which is also common to accentuate the deflection. When combined with a thick nanocrystalline coating of substantially higher strength, there is a significant likelihood that the substrate can relieve the stress it is intended to measure by deforming plastically. Such complexities render the extraction of a stress value a qualitative exercise at best.

The family of approaches that directly measures the fine, microscale deflections associated with deposition over thick, relatively rigid substrates can in principle overcome the issues described above. Small deflections eliminate concerns about the time-dependence of the current density distribution, while thick substrates mitigate the possibility of plastic deformation. For example,

laser-based curvature measurements of a substrate before and after deposition are eminently viable for the study of very thin nanocrystalline films [24-29]. However, the requirement of a reflective surface limits the thickness range that is accessible; thicker electrodeposited coatings (between 10-100 μm) of the kind used widely in industrial applications do not typically retain a mirror finish, and the typical finishes (which range from matte to rough) scatter the incident laser and render curvature measurements impossible. While the addition of so-called levelers or brighteners to induce a mirror surface finish may be possible with some specific electrodeposition baths, these additives can also generally be expected to modify the internal stress of the coating and, therefore, undermine the goal of the experiment.

In light of these issues, the residual stress state in nanocrystalline electrodeposits has rarely been studied in any systematic fashion, particularly for thicker coatings of the finest nanoscale grain sizes. Given the rapid increase in the use of electrodeposited nanocrystalline coatings in industry, there is a growing need to address this issue in a general sense as well as for specific electrodeposited materials. It is the purpose of this paper to systematically assess the residual stress in nanocrystalline Ni-W alloy electrodeposits of large thicknesses (10-100 μm) and from a bath without levelers or brighteners. We develop a straightforward procedure that involves a specific plating geometry in combination with three-dimensional profilometry, permitting reasonable quantitative stress measurements. We also explore the effects of subsequent annealing on the evolution of residual stress and offer insight into the physical origins of the intrinsic stress in Ni-W deposits.

2. Electrodeposition of Nanocrystalline Ni-W

Nanocrystalline Ni–W specimens were electrodeposited from an aqueous solution based on an approach developed and described in detail in Ref. [12]. All specimens were deposited onto copper substrates of commercial purity using a platinum mesh counter electrode with a spacing of approximately 7.6 cm between the electrodes. Table I provides the composition of the plating bath, whose temperature and pH were maintained at 75 ± 2°C and 7.4 ± 0.05, respectively. Deposition was conducted in a 4 L beaker, with continuous stirring at a rate of 200 rpm. Ammonium hydroxide additions were used to adjust the pH when necessary.

TABLE I. Plating bath composition used for specimen preparation

Chemical name and formula	Concentration (g/L)
Nickel sulfate hexahydrate ($NiSO_4 \cdot 6H_2O$)	15.8
Sodium tungstate dihydrate ($Na_2WO_4 \cdot 2H_2O$)	46.2
Sodium citrate dihydrate ($Na_3C_6H_5O_7 \cdot 2H_2O$)	147.1
Ammonium chloride (NH_4Cl)	26.7
Sodium bromide (NaBr)	15.4

The electrodeposition technique employed here uses pulsed current waveforms to tailor the composition and grain size of the deposit, after Ref. [12]. We used a fixed forward (cathodic) baseline current density of 0.2 A/cm^2 of 20 ms duration, to which we introduced a periodic 3-ms pulse ranging in amplitude (A_p) from 0 (direct current) to 0.5 A/cm^2, as depicted in Fig. 1a. Note that the amplitude of the pulse is sometimes sufficiently large that the pulse is anodic (i.e., when A_p is greater than the cathodic baseline of 0.2 A/cm^2), can also describe conventional pulse plating with off-time (i.e., when A_p is equal to 0.2 A/cm^2), and involves a secondary, lower cathodic current when the amplitude is small (i.e., when A_p is less than 0.2 A/cm^2).

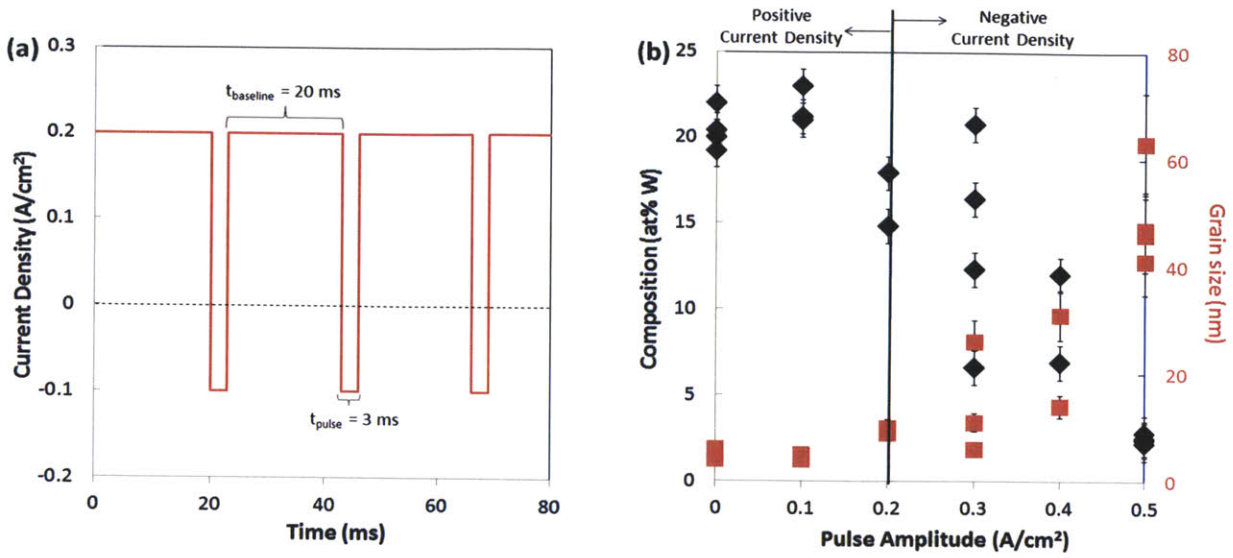

Figure 1: (a) The current waveform applied in this work consists of a fixed forward (cathodic) baseline current density of 0.2 A/cm^2 of 20 ms duration coupled with a 3-ms pulse ranging in amplitude from 0 (direct current) to 0.5 A/cm^2. (b) Pulses with larger amplitudes lead to lower W content and because the solute atoms have a slight tendency to segregate to the grain boundary in the Ni-W system, a finer grain size is thermodynamically preferred for deposits with higher W contents. Pulse amplitudes greater than 0.2 A/cm^2 correspond to negative currents and the removal of atoms.

During the cathodic current periods, both Ni and W are deposited in a fixed ratio (with less W incorporation occurring at lower current densities) whereas W is selectively removed during periods when the current is negative as a result of its higher oxidation potential [12]. Each baseline period of 20 ms corresponds to the deposition of material with a volume roughly equivalent to a single monolayer. As a result, as illustrated in Fig. 1b, pulses with larger amplitudes lead to lower W content being incorporated into the deposit. Since W exhibits a slight tendency to segregate to the grain boundaries in Ni [30], increasing the concentration of W promotes an increase in the total grain boundary area and, thus, drives the system towards finer grain sizes as seen in Fig. 1b. The processing conditions described above were used to produce 10-100 μm thick films with grain sizes (compositions) ranging from 4 nm (23 at.%W) to 63 nm (2 at.%W).

Traditional metallographic techniques were used to prepare and mechanically polish cross-sections of the deposited films. Film thickness and composition (to within ±1 at.%) were measured using a Leo 438VP scanning electron microscope (SEM) operating at 20kV and fitted with a calibrated energy dispersive spectroscopy (EDS) detector. A PANalytical X'Pert Pro diffractometer with a Cu Kα radiation source operating at 40 mA and 45 kV was used to obtain X-ray diffraction (XRD) peak profiles for the as-deposited films. After identifying the peak positions and calculating the full-width at half-maximum peak widths using the Jade software package (MDI, Inc., Livermore, CA), the grain sizes were quantified to within ±15% by applying the Scherrer equation [18] to the (111) peak. Instrumental broadening effects were removed using the Cauchy-Gaussian approach [31]. This grain size analysis technique has been shown to be accurate for Ni-W alloys [10], where the measured XRD grain sizes were verified by extensive transmission electron microscopy (TEM).

3. Elastic Property Measurements

A separate set of films were prepared for the specific purpose of assessing the elastic properties of the alloys by nanoindentation for incorporation into the residual stress calculations. A Hysitron Ubi1 indenter with a diamond Berkovich tip was employed, and all tests were performed at a constant indentation strain rate under a constant applied maximum load of 10 mN, corresponding to depths in the range of 200-250 nm. After loading at the strain rate of interest, the sample was unloaded to 20% of the maximum load and a 10 s hold was used to characterize instrumental drift. A minimum of 30 indentation curves were used to calculate each of the reported modulus values.

The Oliver-Pharr method [32] was used to determine the reduced modulus, E_r, from load-displacement curves, using a tip area function that was carefully calibrated on fused silica. Reduced modulus values were measured at seven indentation strain rates between $1.5 \cdot 10^{-2}$ to 15 s^{-1} and the results are plotted against strain rate in Fig. 2, demonstrating that no significant trend is apparent. Thus, an average reduced modulus value over all strain rates is used for each grain size in the subsequent analyses.

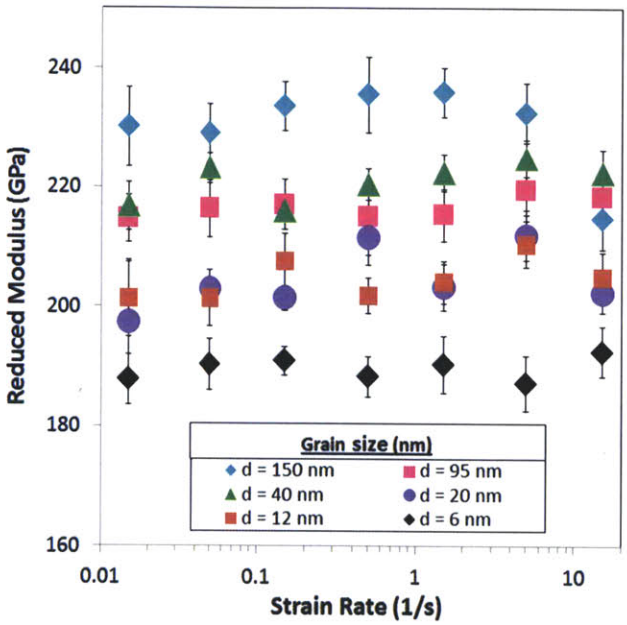

Figure 2: Reduced modulus as a function of strain rate, as measured by nanoindentation. No significant trend with strain rate is apparent over the range of $1.5 \cdot 10^{-2}$ to 15 s^{-1}.

The reduced modulus is a composite elastic parameter that incorporates properties of both the film and the diamond indenter tip, according to [32]:

$$\frac{1}{E_r} = \frac{1-\upsilon_f^{\,2}}{E_f} + \frac{1-\upsilon_i^{\,2}}{E_i} \quad (1)$$

where E is Young's modulus and ν is Poisson's ratio, and the subscripts i and f refer to the properties of the diamond indenter and the Ni-W film, respectively. Equation 1 can be used to extract the Young's modulus of the Ni-W film from the measured values of E_r. We assumed a

value of $\nu_f = 0.31$ for the Ni-W films and used the standard literature values of $\nu_i = 0.07$ and $E_i = 1141$ GPa for diamond [33].

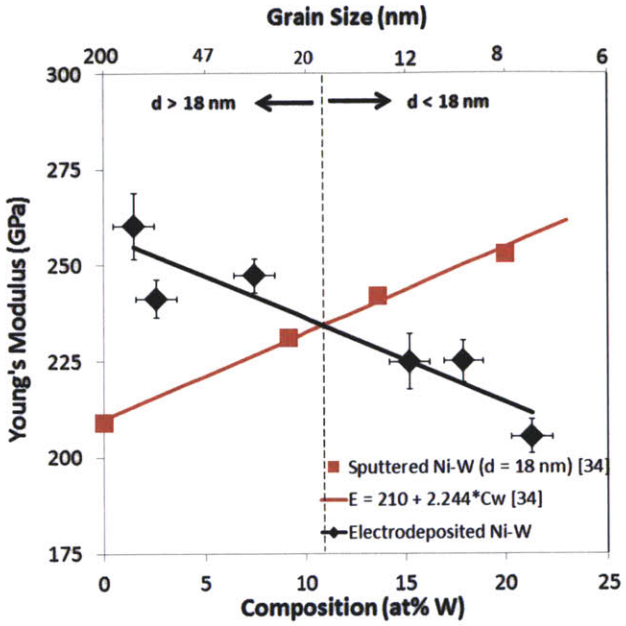

Figure 3: Plotting Young's modulus for the electrodeposited Ni-W films reveals a decrease in E as a result of increased W content coupled with decreased grain size. For comparison, the results from a study of magnetron sputtered Ni-W [34], where the grain size was kept constant at $d = 18$ nm, are also plotted.

Fig. 3 plots the resulting Young's modulus values as a function of composition. An increase in Young's modulus with alloying might be expected as a result of the stiffer bonds of pure W ($E = 402$ GPa) as compared to pure Ni ($E = 207$ GPa). Indeed, Rupert et al. observed a linear increase in modulus with increasing W content, also plotted in Fig. 3, for magnetron sputtered Ni-W films with a constant grain size of 18 nm [34]. However, in our present work, the grain size is not constant and can be expected to contribute an additional complicating factor to the effective modulus value. For clarity, the corresponding measured grain sizes are provided on the top of Fig. 3. Where our grain sizes are smaller than the 18 nm used in Ref. [34], we observe a negative shift in E from their reported results. It is reasonable to suggest that the increased volume fraction of grain boundaries, where we might expect dilated, more compliant bonds

between atoms, associated with these smaller grain sizes, may account for this discrepancy. Previous studies have observed a similar deleterious effect on modulus with decreasing grain size [1, 35, 36]. Conversely, a small positive shift in E may be expected for grain sizes larger than the 18 nm used in Ref. [34]; however, if even discernible, this grain size effect would be far more diminished than that observed in Fig. 3, as the volume fraction of grain boundaries would be relatively constant in this regime.

4. Residual Stress in the Electrodeposits

Our approach to stress measurement is based upon profilometry curvature measurements. To ensure axisymmetric elastic properties, and thereby an equibiaxial stress, within the plane of the substrates, it is important to recognize that copper (our substrate material) is significantly elastically anisotropic. Through experimentation, it was found that copper sheet metal (with a rolling texture [37]) could not be used effectively as a substrate in our experiments due to the in-plane anisotropy of its elastic properties and anisotropic curvature development upon electroplating. To address this issue, copper disks of approximately 0.5 mm thickness were cut from an extruded 2.54-cm diameter cylindrical rod. The extrusion texture for copper is transversely (in-plane) isotropic, as are the resulting curvatures. The copper disks were mechanically polished to 800 grit, electropolished, and then electrocleaned to provide a smooth, uniform surface for plating.

Although it is common to use the linearized Stoney formula for residual stress calculations based on curvature measurements, the conditions under which it is valid (a coating to substrate thickness ration of ~5% [13]) are quite restrictive, and often involve deflections below the viable

resolution of profilometry. Accordingly, we employ the extended Stoney formula for thick films [13, 38] to determine the average residual stress, σ, from the change in curvature, ΔK, of the substrate before and after deposition:

$$\sigma = \frac{M_s h_s^2}{6h_f} \Delta \mathrm{K} \frac{1 + 4HM + 6H^2M + 4H^3M + H^4M^2}{1 + H} \qquad (2)$$

where M_x and h_x represent the biaxial modulus and thickness of the substrate (x = s) or film (x = f), respectively, while M and H refer to a ratio of the film to the substrate property. Film thickness was calculated from an average of nine thickness measurements along the center one-third region during SEM characterization, and substrate thickness was measured at five locations using a micrometer and then averaged.

Based on the Young's modulus data presented in Fig. 3, values for the biaxial modulus were calculated using the following formula [13]:

$$M_f = \frac{E_f}{1 - \upsilon}. \quad (3)$$

As noted earlier, the extrusion texture for copper is transversely isotropic, and Schmid and Wassermann found that that the preferred orientation of extruded pure copper metal parallel to the fiber axis has a relative proportion of 40 vol% <100> and 60 vol% <111> [37].

The effective biaxial moduli for the (100) and (111) planes for copper were calculated as 114.8 GPa and 261.0 GPa, respectively, from [13]:

$$M_{001} = C_{11} + C_{12} - \frac{2C_{12}^{\ 2}}{C_{11}} \quad (4)$$

$$M_{111} = \frac{6(C_{11} + 2C_{12})C_{44}}{C_{11} + 2C_{12} + 4C_{44}} \quad (5)$$

where the elastic constants for copper are taken to be C_{11} = 168.4 GPa, C_{44} = 75.4 GPa, and C_{12} = 121.4 GPa [33]. A simple rule-of-mixtures using these values yielded a value of 202 GPa for the effective biaxial modulus, M_s, of the extruded copper rod substrate material.

To measure the curvature change associated with deposition, three-dimensional traces of the center one-third region of the sample surface, represented by the image in Fig. 4, were obtained using a KLA-Tencor P-16+ profilometer (Milpitas, CA, USA) equipped with a 2 μm stylus. Three-dimensional profilometry provides a more robust analysis method as compared to its two-dimensional counterpart, ensuring that the maximum curvature is always measured.

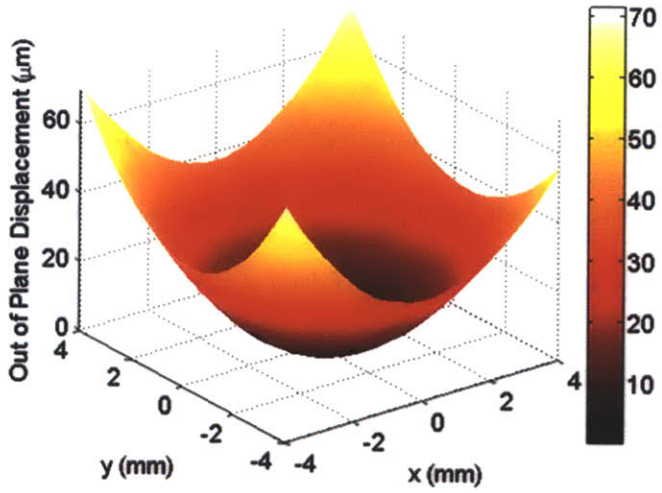

Figure 4: A representative three-dimensional profilometry trace of the center one-third region of a copper substrate.

A non-linear least squares approach was used to fit an ellipsoid to the sample surface, and the mean curvature of the ellipsoid, K, was calculated at its vertex $(0,0, z_o)$:

$$K = \frac{abc(a^2 + b^2)}{2a^3b^3} \quad (6)$$

where $a, b,$ and c are the fitted ellipsoid radii.

An important obstacle to the use of the extended Stoney formula with electrodeposits is achieving a uniform film thickness, h_f, which is complicated by a non-uniform current density distribution that results in thicker deposits near the edges of the substrate, known commonly as the "edge effect". The reason this thickness non-uniformity is of concern is that a portion of the resulting measured curvature of the substrate would result not from the true bending of the substrate but instead from the increasing film thickness found in moving from the center of the film towards its edges.

To improve the current density distribution over the surface area of the substrate, an auxiliary cathode (or current thief) was constructed [39]. Copper wire of 0.4 mm diameter was electrically connected to the substrate and positioned around its perimeter at a constant offset distance of 1 mm, as depicted in Fig. 5. Note that the full area of the substrate and the thief were taken into account when calculating the necessary current to apply to obtain the current density waveform illustrated previously in Fig. 1. The current thief redistributes the electric field near the edges of the substrate, leading to a significantly more uniform deposit near the substrate edges, as seen in Fig. 6.

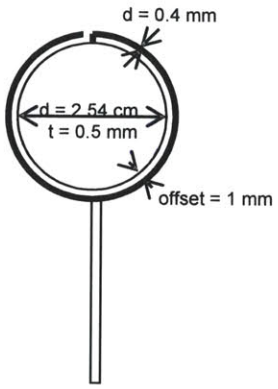

Figure 5: Dimensions of copper substrate and copper wire current thief around its perimeter. The thief improves the current density distribution across the substrate surface, resulting in a more uniform deposit.

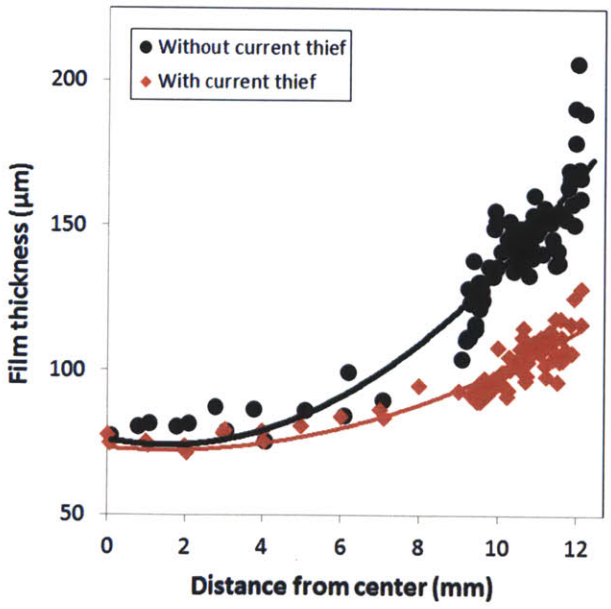

Figure 6: Cross-sectional view of the radius of two DC-plated Ni-W films of approximately 75 µm thickness illustrating an increasing film thickness in moving from the center (0 mm) to the edge of the films (12.7 mm). It is clear that the addition of a current thief significantly improves the deposit uniformity, particularly in the region closest to the edge.

The residual stress was characterized for 16 samples deposited using processing conditions ranging in pulse amplitude from 0-0.5 A/cm^2 with resulting compositions, grain sizes, and thicknesses varying from 2-23 at% W, 4-63 nm, and 10-98 μm, respectively. Table II summarizes the conditions used to produce each specimen.

TABLE II. Processing conditions and characterization of electrodeposited Ni-W films

Pulse amplitude (A/cm^2)	Thickness (im)	W Content (at%)	XRD Grain size (nm)	Post-9h anneal XRD Grain size (nm)	As-deposited stress (MPa)
0	11	20	6		507
0	10.6	20.4	6		500
0	25	22	4		477
0	77	19.2	5		361
0.1	11.3	21	5	5	799
0.1	21.3	21.2	4	4	474
0.1	75	23	4	4	393
0.2	11.5	17.9	9		1018
0.2	22.9	14.8	10		1096
0.3	11	6.6	26		689
0.3	21.4	12.3	11		876
0.3	98.3	20.8	6	6	553
0.4	12.7	6.9	31		769
0.4	23.2	12	14		1227
0.5	14.1	2.2	63		198
0.5	29.4	2.4	47		523

In order to determine the intrinsic residual stress state of the films, the extrinsic stress due to the difference in thermal contraction between the material being deposited (Ni-W) and the substrate (Cu) as the films cooled from the deposition temperature of 75°C to room temperature was first calculated and subtracted out. The extrinsic stress was found to vary from 77-90 MPa (compressive) using the following relationship [40]:

$$\sigma_{extrinsic} = M_f(\alpha_s - \alpha_f)(\Delta T) \quad (7)$$

where thermal expansion coefficients, α, of $16.5 \cdot 10^{-6}$, $13.4 \cdot 10^{-6}$, and $4.50 \cdot 10^{-6}$ K^{-1} [41] were used for Cu, Ni, and W, respectively, and a rule of mixtures was applied to estimate the thermal expansion coefficient of the films.

The resulting intrinsic residual tensile stress in these as-deposited Ni-W films was found to vary from approximately 300-1300 MPa across this experimental space as illustrated in Fig. 7a.

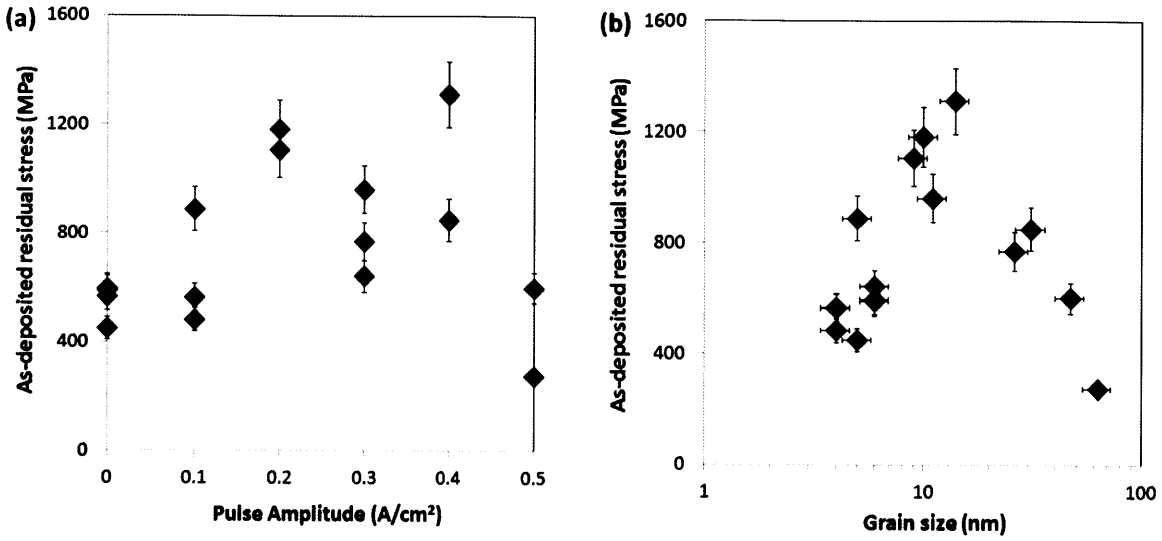

Figure 7: a) The intrinsic residual stress of the as-deposited Ni-W films ranges from approximately 300-1300 MPa for pulse amplitudes ranging from 0 to 0.5 A/cm^2. b) Re-plotting this data as a function of grain size in a semi-logarithmic fashion better represents the range of accessible grain sizes. A rapid increase in residual stress occurs with an increase in grain size below ~20 nm while further increases in grain size result in a gradual decrease in stress.

Figure 7a compiles all of the experimental data on a single axis related to a processing variable, but the data show a great deal of scatter and no obvious trend with this single parameter. We attribute this to the complex interdependency of processing conditions, grain size, and composition, and note that the data in Fig. 7a correspond to different thickness coatings as well. As a result, presenting the data in this raw form obscures the important physical trends. In Fig. 7b, we replot the same data as a function of grain size (using a semi-logarithmic scale to better represent the range of accessible grain sizes). We now observe a strong and reproducible trend wherein the stress level appears to first increase rapidly with grain size for the smallest grain sizes (<15 nm) and then gradually decreases beyond this point.

5. Residual Stress Evolution during Annealing

In order to investigate the evolution of the stress state, the Ni-W films were annealed at 200°C. Intermittently, after 1, 2, 4, 6, and 9 hours, the films were cooled back to room temperature and their curvatures were measured in order to determine the residual stress using the approach outlined earlier. In all of the samples, the resulting stress levels were found to increase significantly in the first 1-2 hours of annealing and then gradually reached a plateau as shown for some typical films in Fig. 8; no significant change in stress was observed for longer times. No evidence of grain coarsening has been observed in these alloys when they are annealed for 24 hours at temperatures up to 300°C [42]. In the present work, the grain size of select samples was measured before and after annealing, verifying this expectation, and the results are provided in Table II.

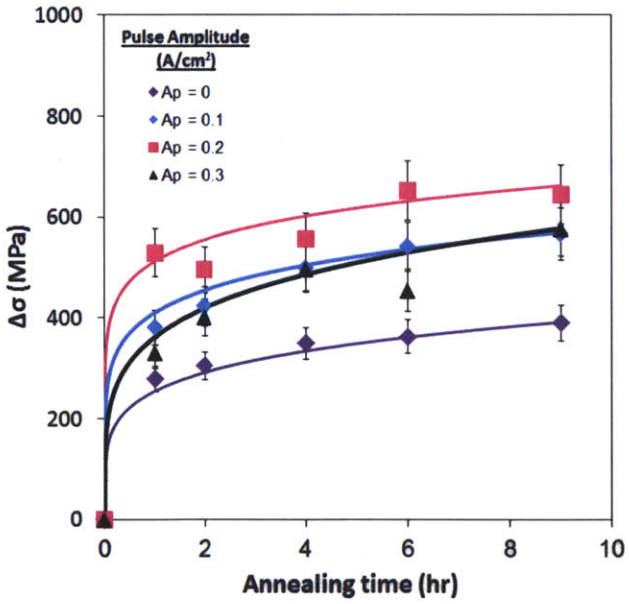

Figure 8: Representative curves showing the evolution of residual stress in the Ni-W films. A significant increase in stress occurs within the first 1-2 hours of annealing at 200°C and eventually a plateau is reached. No significant increase in stress is apparent after 9 hours of annealing.

The total increase in stress at the exhaustion of the annealing process can be extracted from Fig. 8 and is plotted in Fig. 9a. The maximum residual stress of the films (taken as the plateau stress value after 9h of annealing at 200°C) is plotted together with the as-deposited stress level in Fig. 9b. In both cases, significant increases are again apparent as the grain size increases up to 15 nm, with a gradual decrease occurring for further increases in grain size. The similar trend in all three cases suggests that a similar mechanism for stress-generation might be at play during both the deposition process and post-processing annealing. This is a point we will return to in the discussion.

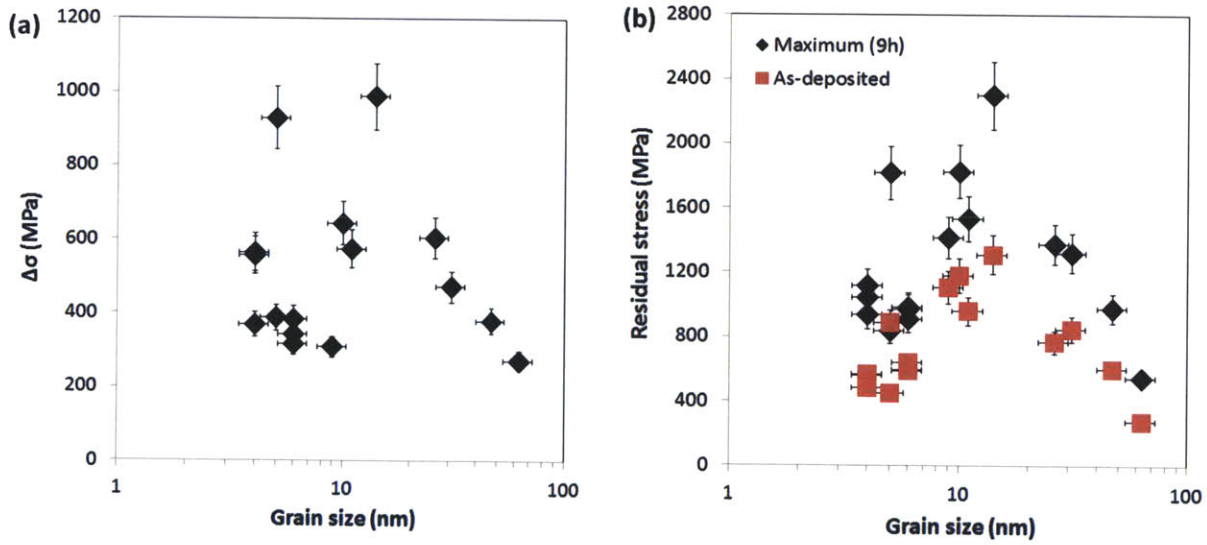

Figure 9: a) The increase in residual stress occurring during the annealing process ranges from approximately 300 to 1000 MPa and b) the maximum residual stress of the annealed Ni-W films ranges from approximately 600 to 2400 MPa for grain sizes between 5-60 nm.

6. Physical Origins of Residual Stress

The above results demonstrate that significant tensile residual stress can be present in nanocrystalline Ni-W in the as-deposited state and that this stress state can also evolve upon annealing. These data also exhibit interesting trends with respect to processing conditions and grain size, and these trends may provide some clues as to the origin of the residual stresses and their evolution and may also potentially point the way to controlling or reducing residual stress in an application setting.

The underlying principle for all of the intrinsic stress generation theories is that while an unconstrained film would shrink as a result of a volume decrease $\Delta V/V$ in the film, its attachment to a substrate forces the build up of a tensile stress, $\Delta\sigma$, to oppose this strain [40]:

$$\Delta\sigma = M_f \cdot \frac{1}{3} \cdot \frac{\Delta V}{V} \quad (8)$$

There are many ways in which the volume of a film might change relative to the substrate. In what follows, we explore some possible physical explanations for the residual stress in the Ni-W system.

6.1 Evolution of Residual Stress During Annealing

6.1.1 Co-deposited Hydrogen Evolution

One prominent theory for the origin of residual stresses in electrodeposits in the literature proposes that co-deposited hydrogen is trapped in the deposits during deposition; its subsequent release therefore decreases the occupied volume of the specimen, creating tensile stress in the

deposit [19]. Hydrogen that evolves from the specimen during plating can thus in principle be associated with the as-deposited residual stress, while stress evolution after deposition or during annealing can be explained by hydrogen removal well after deposition. Nickel-based deposition processes are known to generally involve hydrogen incorporation [43-45], and the present Ni-W specimens are no exception. Select deposits were placed in a beaker of glycerin heated to 100°C immediately after deposition, upon which hydrogen evolution was directly observed; a prodigious number of small bubbles (~100, 1 mm diameter) were emitted from the specimen before gas evolution slowed and ceased after about 10 minutes. An identical set of deposits were allowed to outgas under vacuum at 0.2 mbar for 22 hours at room temperature, which was found to release all of the hydrogen without requiring a thermal treatment; samples subjected to the vacuum conditions released essentially no gas upon subsequent immersion in 100°C glycerin. No observable difference in the hydrogen content for different processing conditions was apparent.

Next, to determine whether the released hydrogen gas could be responsible for the observed volume shrinkage and resulting increase in stress occurring during annealing, three Ni-W films of varying thickness and current waveform parameters were prepared: A_p = 0.1 A/cm^2, h_f = 21 μm; A_p = 0.1 A/cm^2, h_f = 75 μm; and A_p = 0.3 A/cm^2, h_f = 98 μm. The curvature of each of these samples was analyzed by profilometry immediately after plating, and then again after experiencing 22 hours in vacuum (a treatment that, as shown above, removes all of the hydrogen without requiring a thermal treatment).

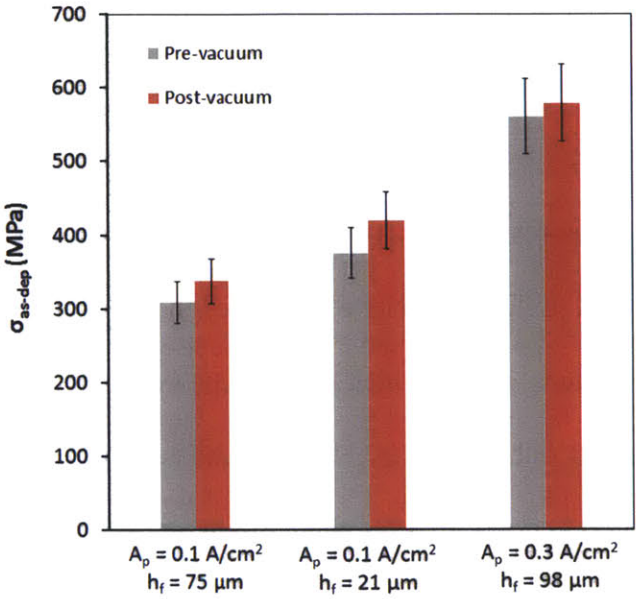

Figure 10: Only a slight increase in residual stress (~15-45 MPa) is observed following the removal of co-deposited hydrogen by outgassing under vacuum at 0.2 mbar at room temperature for 22 hours. These results suggest that the post-deposition release of hydrogen plays a very minor role in the final residual stress state of electrodeposited nanocrystalline Ni-W films and would not be responsible for the large volume shrinkage observed following annealing.

As shown in Fig. 10, in all three cases, we observe only a negligible change in residual stress (~15-45 MPa) following the removal of co-deposited hydrogen; this change is well within the error of the measurement (± 10%), and is smaller by an order of magnitude or more than the as-deposited residual stress. This value is also far smaller than the additional increment of residual stress $\Delta\sigma$ that is found to develop upon annealing (cf. Fig. 9a). Accordingly, we conclude that the post-deposition release of hydrogen plays a very minor role in the final residual stress state of annealed nanocrystalline Ni-W films. Although we cannot strictly rule out a contribution of hydrogen evolution during deposition to the as-deposited residual stress, the fact that we observe no clear differences in hydrogen evolution among the various specimens, despite very large differences in their residual stress state, suggests that hydrogen plays a minor role at best.

6.1.2 Structural Rearrangements and Defect Annihilation

The densification of films as a result of the coalescence of isolated deposition clusters is a widely cited theory of stress generation in the literature [46-52]; however, while this may be the most significant stress-producing process to occur in very thin, non-continuous films, it is not clear why it would apply to the relatively thick films (10-100 μm thick) deposited in our study. This mechanism leads to a maximum tensile stress occurring at the point when the film first becomes completely continuous (at <100 nm thickness) followed by a gradual reduction and eventual leveling off of tensile stress at a film thickness of around 200 nm [50]; with thicknesses several orders of magnitude beyond this transition, we need to consider alternative mechanisms for the present Ni-W coatings. Another prominent stress generating mechanism common in very thin films but also not especially relevant to our current study is the growth of a film with an epitaxial relationship to the substrate where a mismatch between the lattice spacings of the two materials is present. The strain energy in the film increases with the thickness of this epitaxial layer until the formation of a series of misfit dislocations at the interface becomes more energetically favorable. In the present case, new nanocrystalline grains are formed every few nm, and at thicknesses of 10-100 μm, a great many grains separate the surface from the substrate; the epitaxial relationship or lack thereof at the substrate interface is not expected to be of great consequence for the bulk of the film.

For the case of continuous metal films, the models of Klokholm and Berry [53] and Buckel [54] suggest that material is deposited in a non-equilbrium state and that subsequent atomic rearrangement (which would result in a shrinkage of the film if it were not attached to the substrate) generates the observed tensile stress. These atomic rearrangements serve to increase

the elastic strain energy while decreasing the total energy of the system. The annihilation of excess vacancies, dislocations, and grain boundaries, phase transformations, precipitation, and compositional changes can all lead to densification volume changes.

6.1.2.1 Grain Growth

Elimination of grain boundaries by grain growth produces a denser material because the atomic density within grain boundaries is less than that in the matrix and would therefore lead to volume shrinkage if the film were not attached to the substrate [55]. This would be especially relevant in nanocrystalline material, where the volume fraction of grain boundaries is very high but changes rapidly over a narrow span of grain sizes. However, grain coarsening is not observed in Ni-W alloys for annealing temperatures up to 300°C for 24 hours [42]. The grain size of select samples in our study was measured before and after annealing to verify this expectation as seen in Table II. As a result, we can eliminate grain growth as a possible mechanism for the stress evolution observed (cf. Fig. 8).

6.1.2.2 Phase Transformations and Particle Precipitation

Volume changes associated with phase transformation and particle precipitation can also result in stress generation in thin films. For example, phase transitions from an amorphous to crystalline structure often result in a 1 to 2% increase in density [56] and the generation of large stresses. However, there is no evidence of phase transformations or particle precipitation in Ni-W films at the temperatures of 200°C and below.

6.1.2.3 Lattice vacancy annihilation

Since deposits are out of equilibrium, they are expected to contain excess vacancies, and their subsequent removal is a densifying proposition. The process of removing atoms from the grain

boundary to annihilate vacancies in the grain interiors would leave gaps at the grain boundaries that would zip together to keep the surfaces of the adjoining crystals together; the constraint of the substrate leads to the development of a biaxial tensile stress. Typically, the vacancy volume is less than the atomic volume (in some cases it may be as small as one half the atomic volume), so when a vacancy annihilates, an associated relaxation of the lattice corresponding to a volume expansion also occurs. Doerner and Nix calculated the stress in Ni from vacancy diffusion and annihilation at grain boundaries for a grain size of 30 nm and an initial vacancy volume fraction of 1% for a range of temperatures and times [40]. After 9 hours at 200°C (similar to our annealing treatment), the calculated stress values were only on the order of 1 MPa (much less than the stress levels observed in our study). If the vacancy relaxational effects noted above were also taken into account, the biaxial tensile stresses would be even smaller. Therefore, it appears unlikely that lattice vacancy diffusion contributes significantly to stress generation in our films.

6.1.2.4 Grain boundary Densification

One of the most widely quoted models of intrinsic stress is Hoffman's grain-boundary relaxation model [48, 49, 57]. According to this model, crystallites that form on a substrate are located at arbitrary positions and result in grain boundaries that are more widely spaced than equilibrium boundaries. As the atoms relax toward their equilibrium positions, an elastic strain and corresponding intrinsic tensile stress develops in the film. Hoffman and others have suggested that the energy change associated with the bonding of two crystallites is given by $(\gamma_{gb} - 2\gamma_s)$, where γ_{gb} is the grain boundary energy and γ_s is the surface energy. They envision that the grain boundary is formed by bringing the surfaces of the two crystallites closer and closer together until they come into contact.

Doerner and Nix argue that it is not appropriate to assume that a major change in the interfacial energy occurs when the crystallites grow together. They offer an alternative picture, one in which the junction between the crystallites is created gradually, one atom at a time, as atoms deposit onto the growing surface of the film [40]. The atoms that are deposited on the top surface of the film either join one of the growing crystallites or reside at one of the grain boundaries. In this way, the nonequilibrium boundary is created one atom at a time and is not formed by the joining of two free surfaces. The resulting picture of many small voids, or grain boundary vacancy clusters, covering most of the grain boundary surface is similar to that of the grain boundary relaxation model proposed by Hoffman.

Doerner and Nix consider that the void surfaces are brought into contact by diffusional processes. Since the energy of the void surface (γ_s) is always greater than the energy of the grain boundary (γ_{gb}), a driving force for void shrinkage exists. In order for the void to shrink, atoms must flow from the grain boundary into the void. Without the substrate constraint, this process of void shrinkage would be accommodated by rigid motion of the two crystals toward each other. Doerner and Nix provide representative results for Ni films at a grain size of 50 nm and a void fraction of 0.003, which is consistent with the samples in our experiments. At temperatures of 75°C and an initial void radius of 2 nm, stress levels of 1.1 GPa would be generated in approximately 8 hours; it is clear that the kinetics are much quicker than that associated with the vacancy annihilation mechanism. These results indicate that for sufficiently small voids and large void volume fractions, grain boundary diffusion can result in reasonable stress generation rates. The general equation for stress evolution by the grain boundary void shrinkage

mechanism that Doerner and Nix derived [40] based on a solution for cavity growth derived by Speight and Beere [58] is as follows:

$$d\sigma = -\frac{M_f}{d}\left[1-\frac{\beta a^3}{\pi R^2 d}\right]\frac{2\pi t D_{gb}\Omega}{\pi R^2 kT}\cdot\frac{\sigma-2\gamma_s/a}{ln\left(\frac{R}{a}\right)-\frac{a^4}{4R^4}+\frac{a^2}{R^2}-\frac{3}{4}}dt \quad (9)$$

where the term $\frac{\beta a^3}{\pi R^2 d}$ represents the volume fraction of voids and D_{gb} is the grain boundary diffusivity, Ω is the atomic volume, k is Boltzmann's constant, γ_s is the surface energy of the void, a is the void radius, $2R$ is the spacing between voids, and β is a geometrical factor dependent on the angle between the void surface and the grain boundary.

6.1.3 Grain Boundary Void Formation and Densification in Ni-W

In the specific case of deposited nanocrystalline coatings, simulation work has shown that vacancies and free volume have a tendency to populate grain boundaries [59]. Ruan and Schuh obtained positive segregation energies for all grain boundary energies employed in their simulation study, with higher segregation tendencies as grain boundary energy increased. They found that vacancies and voids kinetically pin grain boundaries and so grain boundaries migrate until they intersect vacancies or voids.

In addition, for Ni-W alloys in particular, Detor and Schuh [42] used calorimetry, hardness measurements, and atom-probe tomography to provide evidence of grain boundary relaxation initiating at temperatures as low as 100°C and proceeding up to temperatures of greater than 300°C, well before the onset of grain growth, short-range ordering, or precipitation of a Ni_4W intermetallic phase. From these observations and the above discussion, we hypothesize that free

volume trapped in the grain boundaries during deposition and its subsequent shrinkage may be responsible for the increase in stress observed during the annealing process.

6.1.4 Proposed Mechanism for Annealing-Induced Stress Evolution of Ni-W

From the above discussion, we assume that any volume change occurring during annealing will be confined to an elimination of the free volume at the grain boundaries (or an increase in grain boundary density). The intergranular volume fraction, or volume fraction of atoms located at grain boundaries, can be expressed by the following relation [30, 60]:

$$V_{gb} = 1 - \left(\frac{d-t}{d}\right)^{D} \qquad (10)$$

where d is the grain size in nm, t is the grain boundary thickness in nm and is assumed to be 0.5 nm, and D is the dimensionality constant and has a value of 3 for conventional polycrystalline structures. Under the assumption that all of the excess free volume in the film will be found at the grain boundaries, the total volume fraction of excess free volume in the as-deposited film, V_{ex}, would be expected to be proportional to the total grain boundary volume fraction:

$$V_{ex} = F \cdot V_{gb} \qquad (11)$$

where F is a proportionality constant that reflects how much free volume is stored on average in a grain boundary, or how far from equilibrium the boundary is.

Eqs. (10) and (11) describe a simple geometrical effect: since grain boundaries are out of equilibrium and contain excess free volume in deposits, having more grain boundaries means incorporating more free volume. This geometrical effect therefore anticipates that deposition stresses are exacerbated simply by having finer grains (more grain boundaries). On the other hand, there are additional non-geometrical effects of processing that dictate just how far from

equilibrium a grain boundary may be (i.e., how much free volume is stored in it). In other words, the free-volume proportionality constant, F, should be expected to be a function of critical processing parameters. In particular, the pulse amplitude (A_p) represents a strong control variable that relates to the "aggressiveness" of the deposition process in the present case. As A_p is increased, more W atoms are stripped away from the deposit in an increasingly aggressive manner during the pulsing period; therefore, it is reasonable to expect an increase in the number of vacancies or voids created with increasing A_p. Whereas the local defect production may occur anywhere on the surface during a pulse, we envision that any local free volume produced would then migrate to the grain boundary regions, where it can be accommodated. Thus, as a first approximation to capture the effect of processing aggressiveness, we propose that F will linearly increase with A_p:

$$F = F_o + B \cdot A_p \quad (12)$$

Here F_o represents an intrinsic free volume content that would be produced for DC deposition ($A_p = 0$), and B is a proportionality constant. The form of Eq. (12) is speculative, and the two constants, B and F_o, must be treated as fitting parameters. However, we regard this form as the simplest possible model to capture the effects of pulse processing, and as we shall see, it seems to capture the most relevant physical trends.

While Eqs. (10) and (11) capture the geometrical effect and are expressed in nm, Eq. (12) captures the effect of processing and is expressed in A/cm^2. To combine these effects into a single coherent model requires some conversion of the units. In the Ni-W system, the relationship between grain size and tungsten content is well known [12] and can be modeled in a

variety of ways [30]; for our purposes here, it is simplest to employ a semi-empirical power-law to capture this known effect:

$$d = G \cdot {C_W}^n \quad (13)$$

where G and n are 149.74 nm and -1.083, respectively.

Additionally, the effect of pulsing on the incorporated W is known for this system and so the pulse amplitude can be converted into terms of W content (in at%), C_W, as:

$$C_W = L \cdot A_p + C_0 \qquad (14)$$

where the conversion constants L and C_0 are -36.688 cm^2A^{-1} and 22.986, respectively, based on the data presented in Fig. 1b.

Combining Eqs. (8) and (10)-(14), we can now express the expected change in residual stress, $\Delta\sigma$, in a Ni-W film upon annealing out all the excess free volume in the film as:

$$\Delta\sigma = M_f \cdot \frac{1}{3} \cdot \left[B \cdot \frac{\left(\frac{d}{G}\right)^{1/n} - C_0}{L} + F_o \right] \cdot \left[1 - \left(\frac{d-t}{d}\right)^D\right] \qquad (15)$$

where the only adjustable parameters in the model are B and F_o. Values of $B = 0.128$ cm^2A^{-1} and $F_o = 0.019$ were determined by finding the best fit of the equation to the experimental data shown in Fig. 12b. The maximum volume shrinkage, $\Delta V/V$, occurring during annealing is synonymous with the fraction of excess free volume, V_{excess}, stored in the as-deposited film.

The term in the first bracket, or the excess free volume content in the grain boundaries, F, represents the processing contribution to the stress generation while the term in the second

bracket, or the volume fraction of grain boundary area in the film, V_{gb}, represents the structural contribution. These two terms are plotted separately in Fig. 11a, and it is clear that their combination yields the concave downward trend that we previously observed in the data.

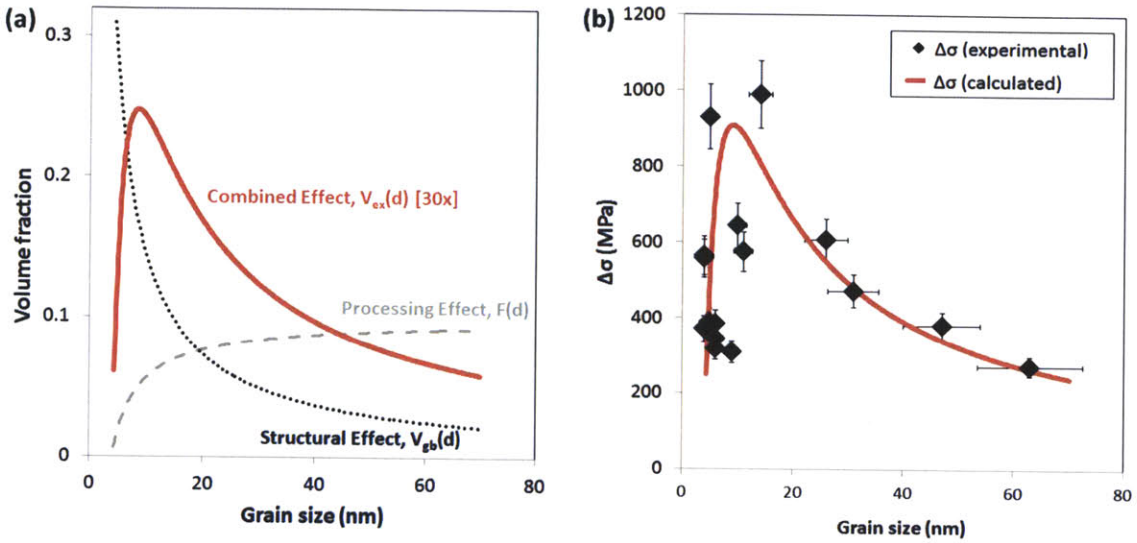

Figure 11: (a) The dashed grey curve represents the calculated excess free volume content in the grain boundaries, *F(d)*, which is controlled by the *processing* parameter A_p while the dotted black curve represents the volume fraction of grain boundary area in the film, $V_{gb}(d)$, which is dependent on the *structural* grain size of the film. Multiplying these two terms together yields the red curve, which represents the bulk excess free volume content of the film, $V_{ex}(d)$, and provides a good indicator of the expected increase in residual stress associated with annealing out this excess free volume. Note that $V_{ex}(d)$ has been multiplied by a factor of 30x for ease of visibility. (b) A comparison of the experimentally-determined $\Delta\sigma$ values as a function of grain size with those values calculated using Eqn. 15.

While on one hand, the increasingly aggressive processing condition (or increasing value of A_p) serves to increase the free volume content in the grain boundaries, on the other hand, the dramatically decreasing grain boundary volume fraction (V_{gb}) structurally limits the amount of free volume that can be stored in the film. This result implies that if less aggressive processing conditions could be used to produce similar grain-sized films, residual stress levels could be reduced. It is also important to note the biaxial modulus term, M_f, is also a function of grain size as evident from Fig. 3; however, modifying M_f results in changes to $\Delta\sigma$ of up to 29%. Compared to changes to $\Delta\sigma$ of up to 1400% by modifying V_{gb} or up to 900% by modifying F, it is clear that

M_f plays a very minor role in residual stress generation over the range of moduli values possible for Ni-W films, and this slight trend does not affect the shape of the combined curve in Fig. 11a.

Furthermore, Fig. 11b reveals the agreement between our fitted values for $\Delta\sigma$ and the experimental observations. The fitting parameter F_o seems very reasonable: it implies that even in the case of DC deposition (where A_p = 0 A/cm^2), the grain boundaries contain approximately 2% excess free volume. As noted in Ref [56], the change in density in transitioning from amorphous to crystalline structures is between 1-2%; therefore, this value is of the order of magnitude that we would expect for disordered grain boundaries.

6.2 Proposed Mechanism for Stress Evolution During Deposition of Ni-W

Returning to the original as-deposited residual stress results, we immediately see a striking resemblance between the shape of the $\sigma_{as\text{-}dep}$ and $\Delta\sigma$ curves -- this correlation is emphasized in Fig. 12, where we plot $\sigma_{as\text{-}dep}$ against $\Delta\sigma$.

This correlation leads us to propose that the shrinkage of grain boundary free volume may also be a prominent factor in the residual stress state of the as-deposited films. In this case, we express the volume decrease due to void shrinkage from the start to end of deposition as $(\Delta V/V)_{dep}$.

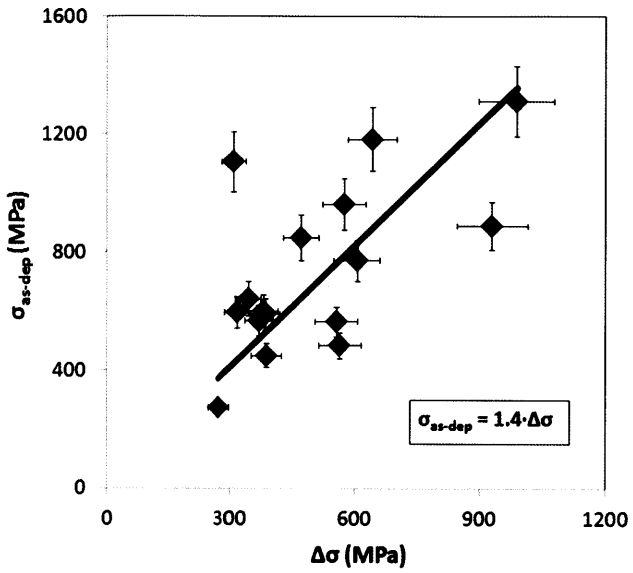

Figure 12: Correlation between the as-deposited residual stress and maximum increase in residual stress upon annealing for the Ni-W films. This relationship points to a similar mechanism of grain boundary free volume also playing a role in the as-deposited stress state.

The ratio between the void volume shrinkage occurring during deposition as compared to that occurring during the annealing process is represented by the factor Q in the following equation:

$$\left(\frac{\Delta V}{V}\right)_{dep} = Q \cdot V_{ex} \qquad (16)$$

where we obtain a value of 1.4 for Q from the empirical relationship presented in Fig. 10.

We then obtain the relationship:

$$\sigma_{as-dep} = 1.4 \cdot M_f \cdot \frac{1}{3} \cdot F \cdot V_{gb} \qquad (17)$$

as shown plotted with good agreement against the experimentally-determined as-deposited residual stress data in Fig. 13.

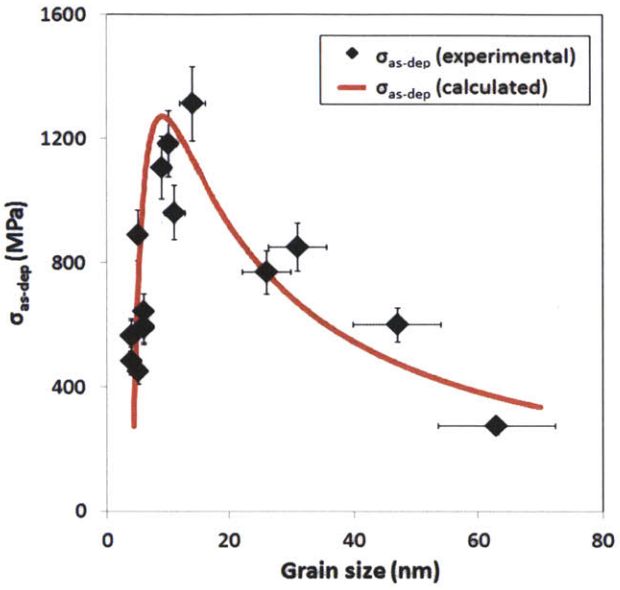

Figure 13: Experimentally-determined and calculated as-deposited residual stress values for electrodeposited Ni-W films ranging in grain size from approximately 5-60 nm. The as-deposited residual stress results from grain boundary void shrinkage occurring during the deposition process. The amount of free volume created and stored in the grain boundaries during the deposition process is set by the pulse amplitude, A_p, which determines the amount of free volume (or voids) created and thereby the percentage of grain boundary volume that will be composed of free volume, and the grain size, d, which determines the volume fraction of grain boundary area.

Doerner and Nix provide an extended discussion on the kinetics of the grain boundary void shrinkage process [40]. Initial void size, void volume fraction, and temperature all play a key role in determining the rate at which this process occurs as seen previously in Eq. (9).

While it may seem odd that more stress is generated during the deposition process (which occurs at 75°C for between 0.25-4 hours depending on the film thickness and conditions used) as compared to the annealing treatment (which occurs at 200°C for 9 hours), there are several factors involved. From the data provided by Doerner and Nix, it is true that an increase of 100°C in temperature would increase the shrinkage rate by roughly a factor of 10^5. However, their calculations also reveal that the void volume fraction plays a significant role in the void shrinkage rate. For an initial void radius of 2 nm at 350 K (similar to the temperature used in our

depositions) and an initial void fraction of 1% in a Ni film, a stress level of 1 GPa is reached in approximately 30 minutes. However, under the same conditions but now with an initial void fraction of 0.2%, it now takes 5.5 hours to reach this same stress level. This effect results because with a larger volume fraction of voids, the voids are closer together and diffusion distances are smaller. Furthermore, initial void radius is also important. Doerner and Nix showed that for a decreased initial void radius, it takes less time to eliminate the void at a given temperature because diffusion distances are again smaller -- decreasing the void radius by a factor of 5 increases the shrinkage rate by around a factor of 10^3.

While the increased temperature of the annealing process may seem to indicate that the void shrinkage process will occur at a faster rate and generate more stress, it is clear that the kinetics are more complicated. One possible explanation for the greater stress generation observed during deposition could be that the film is initially composed of a large void volume fraction (on the order of 1-2%) of both small and large voids. Because the void shrinkage rate for smaller voids is so much greater than that of larger voids, the smallest voids are quickly eliminated, leaving behind only larger voids that are shrunk and eliminated at a much slower rate due to both the decreased volume fraction of voids and their larger radii. Because the deposition process occurs on a layer-by-layer basis, with Ni and W atoms deposited during the 20-ms baseline current period and W atoms being preferentially removed during the 3-ms pulse, this elimination of small voids occurs iteratively. The void shrinkage mechanism continues during the annealing treatment at a faster rate than it left off at (due to the increase in temperature); however, the shrinkage rate will never attain the initial value experienced for the small voids at high void volume fraction present directly following a pulse period of deposition.

7. Conclusions

We have proposed a three-dimensional profilometry-based approach and the application of a current thief that permits a straight-forward quantitative analysis of residual stress of thick nanocrystalline Ni-W electrodeposits.

Residual stresses were produced during both deposition and subsequent annealing. The magnitude of the as-deposited intrinsic residual stress for Ni-W films with grain sizes of ~5-60 nm ranges from approximately 300-1300 MPa (tensile) with a maximum occurring at a grain size of between 10-15 nm. The maximum residual stress values obtained after annealing range from 550-2300 MPa (tensile) with a maximum again occurring at a grain size of between 10-15 nm. An increase of ~70% of the as-deposited residual stress can be expected upon heat treatment.

The residual stress of the as-deposited film is determined primarily by the fraction of free volume (or voids) in the grain boundaries of the film. The amount of free volume created and stored in the grain boundaries during the deposition process can be predicted by both the pulse amplitude, which determines the amount of free volume (or voids) created and thereby the percentage of grain boundary volume that will be composed of free volume, and the grain size, which determines the volume fraction of grain boundary area. As a result of subsequent grain boundary void shrinkage, a tensile stress develops in the film in order to compensate for the desired volume decrease while still maintaining the substrate dimensions.

The same mechanism of grain boundary void shrinkage (or an increase in the density of the grain boundaries) is responsible for the increase in residual stress occurring during subsequent annealing.

8. Future Work

Several paths could be taken to extend the research conducted in this thesis:

1) Possible approaches to reduce the residual stress in Ni-W films could be explored. For instance, Ruan and Schuh have shown that increasing the deposition rate decreases the ratio of volume-conserving to non-volume conserving events, thus causing the vacancy (or free volume) content to increase [59]. In addition, they observed that the effect of temperature on free volume content appeared to be negligible. Therefore, an effort to deposit similar structures using baseline current densities that yield lower deposition rates may be one method to effectively reduce residual stress levels. Alternatively, the use of levelers and brighteners to deposition baths is well-known to reduce the residual stress state of electrodeposits. With the added knowledge that the residual stress state is largely controlled by the formation of free volume in the deposit, a more scientific understanding of the use of these additives could be attained.

2) For industrial applications, further exploration of the kinetics of the stress generation process at both room and elevated temperatures may be of interest in determining the maximum stress levels expected at any annealing temperature-time combination.

3) For fundamental science applications, it may be of interest to experimentally study the stress generation rates for temperatures above which grain growth occurs (above 300°C), where we expect that a different stress generation mechanism will be active.

4) Our current knowledge of residual stress in single layer nanocrystalline Ni-W films provides a solid basis from which to investigate the stress state in bi-layered, multi-layered, or

functionally graded film structures either experimentally or through modeling. Such studies would help to provide an understanding of the processing issues associated with residual stress development between mismatched layers. The role of layer thickness and grain size ratios could be explored and the distribution of stresses as more distinct layers are added to the system could be determined.

References

[1] Gleiter H, *Nanocrystalline materials*, Progress in Materials Science, **33**, 223 (1989)

[2] Tjong SC, Chen H, *Nanocrystalline materials and coatings*, Materials Science & Engineering R-Reports, **45**, 1 (2004)

[3] Kumar KS, Van Swygenhoven H, Suresh S, *Mechanical behavior of nanocrystalline metals and alloys*, Acta Materialia, **51**, 5743 (2003)

[4] Grossinger R, Sato R, Holzer D, Dahlgren M, *Properties, benefits, and application of nanocrystalline structures in magnetic materials*, Advanced Engineering Materials, **5**, 285 (2003)

[5] Jiles DC, *Recent advances and future directions in magnetic materials*, Acta Materialia, **51**, 5907 (2003)

[6] Lu L, Shen Y, Chen X, Qian L, Lu K. Ultrahigh strength and high electrical conductivity in copper. vol. 304, 2004. p.422.

[7] Meyers MA, Mishra A, Benson DJ, *Mechanical properties of nanocrystalline materials*, Progress in Materials Science, **51**, 427 (2006)

[8] Suryanarayana C, *Nanocrystalline materials*, International Materials Reviews, **40**, 41 (1995)

[9] Jones AR, Hamann J, Lund AC, Schuh CA, *Nanocrystalline ni-w alloy coating for engineering applications*, Plating & Surface Finishing, 52 (2010)

[10] Rupert TJ, Schuh CA, *Sliding wear of nanocrystalline ni-w: Structural evolution and the apparent breakdown of archard scaling*, Acta Mater., **58**, 4137

[11] Chianpairot A, Lothongkum G, Schuh CA, Boonyongmaneerat Y, *Corrosion of nanocrystalline ni-w alloys in alkaline and acidic 3.5 wt.% nacl solutions*, Corrosion Science, **53**, 1066

[12] Detor AJ, Schuh CA, *Tailoring and patterning the grain size of nanocrystalline alloys*, Acta Mater., **55**, 371 (2007)

[13] Freund LB, Suresh S. Thin film materials: Stress, defect formation, and surface evolution. Cambridge, UK: Cambridge University Press, 2003.

[14] Drory MD, Thouless MD, Evans AG, *On the decohesion of residually stressed thin-films*, Acta Metallurgica, **36**, 2019 (1988)

[15] Czerwinski F, Kedzierski Z, *On the mechanism of microcrack formation in nanocrystalline fe-ni electrodeposits*, Journal of Materials Science, **32**, 2957 (1997)

[16] Peroulis D, Pacheco S, Sarabandi K, Katehi LPB. Alleviating the adverse stress effects of residual stress in rf mems switches. Proc. Eur. Microwave Conf, 2001. p.173.

[17] Noyan IC, Cohen JB. Residual stress: Measurement by diffraction and interpretation, 1986.

[18] Cullity B. Elements of x-ray diffraction. Reading, MA: Addison-Wesley, 1959. p.262.

[19] Weil R, *The origins of stress in electrodeposits*, Plating, **57**, 1231 (1970)

[20] Dini JW. Electrodeposition. The materials science of coatings and substrates. Park Ridge, NJ: Noyes Publications, 1993.

[21] Kouyumdjiev CN, *Residual-stress distribution by the bending strip method*, Surface & Coatings Technology, **28**, 39 (1986)

[22] Sotirova-Chakarova GS, Armyanov SA, *The internal-stress in ni, nife, cofe, and coni layers measured by the bent strip method*, Journal of the Electrochemical Society, **137**, 3551 (1990)

[23] Stoney GG, *The tension of metallic films deposited by electrolysis*, Proc. R. soc. Lond. Ser. A-Contain. Pap. Math. Phys. Character, **82**, 172 (1909)
[24] Flinn PA, Gardner DS, Nix WD, *Measurement and interpretation of stress in aluminum-based metallization as a function of thermal history*, Ieee Transactions on Electron Devices, **34**, 689 (1987)
[25] Geisz JF, Kuech TF, Lagally MG, Cardone F, Potemski RM, *Film stress of sputtered w/c multilayers and strain relaxation upon annealing*, Journal of Applied Physics, **75**, 1530 (1994)
[26] Pan JT, Blech I, *Insitu stress measurement of refractory-metal silicides during sintering*, Journal of Applied Physics, **55**, 2874 (1984)
[27] Sinha AK, Levinstein HJ, Smith TE, *Thermal-stresses and cracking resistance of dielectric films (sin, si3n4, and sio2) on si substrates*, Journal of Applied Physics, **49**, 2423 (1978)
[28] Volkert CA, *Stress and plastic-flow in silicon during amorphization by ion-bombardment*, Journal of Applied Physics, **70**, 3521 (1991)
[29] Zhao ZB, Hershberger J, Yalisove SM, Bilello JC, *Determination of residual stress in thin films: A comparative study of x-ray topography versus laser curvature method*, Thin Solid Films, **415**, 21 (2002)
[30] Trelewicz JR, Schuh CA, *Grain boundary segregation and thermodynamically stable binary nanocrystalline alloys*, Physical Review B (Condensed Matter and Materials Physics), **79**, 094112 (2009)
[31] Zhang Z, Zhou F, Lavernia E, *On the analysis of grain size in bulk nanocrystalline materials via x-ray diffraction*, Metallurgical and Materials Transactions A, **34**, 1349 (2003)
[32] Oliver WC, Pharr GM, *An improved technique for determining hardness and elastic-modulus using load and displacement sensing indentation experiments*, Journal of Materials Research, **7**, 1564 (1992)
[33] Simmons G, Wang H. Single crystal elastic constants and calculated aggregate properties: A handbook. Cambridge, MA: MIT Press, 1971.
[34] Rupert TJ, Trenkle JC, Schuh CA, *Enhanced solid solution effects on the strength of nanocrystalline alloys*, Acta Mater., **59**, 1619
[35] Latapie A, Farkas D, *Effect of grain size on the elastic properties of nanocrystalline alpha-iron*, Scripta Materialia, **48**, 611 (2003)
[36] Zhou Y, Erb U, Aust KT, Palumbo G, *The effects of triple junctions and grain boundaries on hardness and young's modulus in nanostructured ni-p*, Scripta Materialia, **48**, 825 (2003)
[37] Dillamore IL, Roberts WT, *Preferred orientation in wrought and annealed materials*, Metallurgical Reviews, **10**, 271 (1965)
[38] Freund LB, Floro JA, Chason E, *Extensions of the stoney formula for substrate curvature to configurations with thin substrates or large deformations*, Applied Physics Letters, **74**, 1987 (1999)
[39] Mehdizadeh S, Dukovic J, Andricacos PC, Romankiw LT, Cheh HY, *Optimization of electrodeposit uniformity by the use of auxiliary electrodes*, Journal of the Electrochemical Society, **137**, 110 (1990)
[40] Doerner MF, Nix WD, *Stresses and deformation processes in thin-films on substrates*, Crc Critical Reviews in Solid State and Materials Sciences, **14**, 225 (1988)

[41] Section 12, properties of solids; thermal and physical properties of pure metals. In: Lide DR, editor. Crc handbook of chemistry and physics. Boca Raton, FL: CRC Press, 2011.
[42] Detor AJ, Schuh CA, *Microstructural evolution during the heat treatment of nanocrystalline alloys*, Journal of Materials Research, **22**, 3233 (2007)
[43] Armyanov S, Sotirovachakarova G, *Hydrogen desorption and internal-stress in nickel coatings obtained by periodic electrodeposition*, Journal of the Electrochemical Society, **139**, 3454 (1992)
[44] Dorsch RK, *Simultaneous electrodeposition of nickel and hydrogen on a rotating disk electrode*, J. Electroanal. Chem., **21**, 495 (1969)
[45] Gabe DR, *The role of hydrogen in metal electrodeposition processes*, Journal of Applied Electrochemistry, **27**, 908 (1997)
[46] Abermann R, Koch R, Kramer R, *Electron-microscope structure and internal-stress in thin silver and gold-films deposited onto mgf2 and sio substrates*, Thin Solid Films, **58**, 365 (1979)
[47] Abermann R, Kramer R, Maser J, *Structure and internal-stress in ultrathin silver films deposited on mgf2 and sio substrates*, Thin Solid Films, **52**, 215 (1978)
[48] Doljack FA, Hoffman RW, *Origins of stress in thin nickel films*, Thin Solid Films, **12**, 71 (1972)
[49] Hoffman RW, *Stresses in thin-films - relevance of grain-boundaries and impurities*, Thin Solid Films, **34**, 185 (1976)
[50] Janda M, Stefan O, *Intrinsic stress in chromium thin-films measured by a novel method*, Thin Solid Films, **112**, 127 (1984)
[51] Kinosita K, Maki K, Nakamizo K, Takeuchi K, *Stress in vacuum deposited films of silver*, Japanese Journal of Applied Physics, **6**, 42 (1967)
[52] Nix WD, Clemens BM, *Crystallite coalescence: A mechanism for intrinsic tensile stresses in thin films*, J. Mater. Res., **14**, 3467 (1999)
[53] Klokholm E, Berry BS, *Intrinsic stress in evaporated metal films*, Journal of the Electrochemical Society, **115**, 823 (1968)
[54] Buckel W, *Internal stresses*, Journal of Vacuum Science & Technology, **6**, 606 (1969)
[55] Chaudhar.P, *Grain-growth and stress relief in thin-films*, Journal of Vacuum Science & Technology, **9**, 520 (1972)
[56] Davis LA. Metallic glasses. Materials Science Division of American Society for Metals. Metals Park, Ohio, 1978. p.190.
[57] Pulker HK, *Mechanical-properties of optical films*, Thin Solid Films, **89**, 191 (1982)
[58] Speight MV, Beere W, Met. Sci. J., **9**, 190 (1975)
[59] Ruan SY, Schuh CA, *Kinetic monte carlo simulations of nanocrystalline film deposition*, J. Appl. Phys., **107**, 11
[60] Palumbo G, Thorpe SJ, Aust KT, *On the contribution of triple junctions to the structure and properties of nanocrystalline materials*, Scripta Metallurgica Et Materialia, **24**, 1347 (1990)